https://doi.org/10.2352/ISSN.2470-1173.2019.15.AVM-046

Color Correction for RGB Sensors with Dual-Band Filters for In-Cabin Imaging Applications

Orit Skorka[1], Paul Kane[2], and Radu Ispasoiu[1]
Intelligent Sensing Group, ON Semiconductor, [1]Santa Clara, CA, USA; [2]Rochester, NY, USA

Abstract

Automotive in-cabin monitoring and surveillance imaging applications operate in the visible band during daytime and in the near infra-red band during nighttime. Utilization of the same camera for imaging in both bands is advantageous as it reduces system complexity. This work evaluates four methods for single-camera dual-band imaging that vary by combinations between color-filter array, i.e., RGB and RGB-IR, camera filter, i.e., infrared-cut filter and dual-band filter, and processing pipeline, i.e., standard RGB and RGB-IR. We conclude that the optimal combination is RGB sensor, dual-band filter, standard color imaging pipeline, and a color correction matrix that is optimized for the visible and near-infrared bands. This method holds the net advantage of system simplicity and sufficient image quality in applications where high color accuracy is of a secondary priority.

Introduction

With automotive in-cabin cameras that are used for surveillance and monitoring, during daytime, when the scene is illuminated by the sun, a natural light source, imaging is done in the visible band. During night time, the scene is illuminated by near infra-red (NIR) light-emitting diode (LED) illuminators and imaging is done in the NIR band, which is invisible to the human visual system (HVS). Use of a single camera for dual-band imaging is advantageous as it reduces system complexity.

These days, digital cameras for these applications are based on CMOS image sensors. The light sensitive element in each pixel of a CMOS image sensor array is a silicon photodiode. While the HVS is only sensitive to photons in the visible band, which spans from 400–700 nm, silicon band gap is 1.1 eV, therefore, it is sensitive to photons in the visible and in the NIR bands with wavelength that is up to about 1,100 nm. Figure 1 compares the normalized photopic curve of the HVS, which represents its spectral sensitivity in bright conditions that allow perception of color, to the normalized quantum efficiency curve (QE) of a monochrome CMOS image sensor.

On the one hand, sensitivity of CMOS image sensors to photons in the visible and the NIR bands is beneficial as it enables use of the same camera for dual-band imaging. On the other hand, it can create a problem in visible-band imaging because the color imaging pipeline relies on the HVS response. Image sensor exposure to NIR photons during image capture in the visible band may result in appearance of brightness (luma) and color (chroma) artifacts in the processed image.

At present, there are two main methods for single-camera dual-band imaging. The first is based on a standard Bayer (RGB) image sensor and mechanical system that places an infrared-cut filter (IRCF) in the path of the light during daytime and removes it during nighttime. However, the additional hardware increases system complexity. The second is based on combination of a special color filter that substantially attenuates pixel sensitivity to photons in the visible band and a dual-band filter (DBF), which transmits light in the visible band and in a narrow band in the NIR. The drawback with this method is that it adds system complexity as it requires a special processing pipeline. Furthermore, this method is also likely to result in degradation in metrics that relate to spatial resolution.

This work introduces a solution that allows the use of an RGB sensor with a DBF and a standard color pipeline for single-camera dual-band imaging with color reproduction that is satisfactory for automotive in-cabin monitoring and surveillance applications.

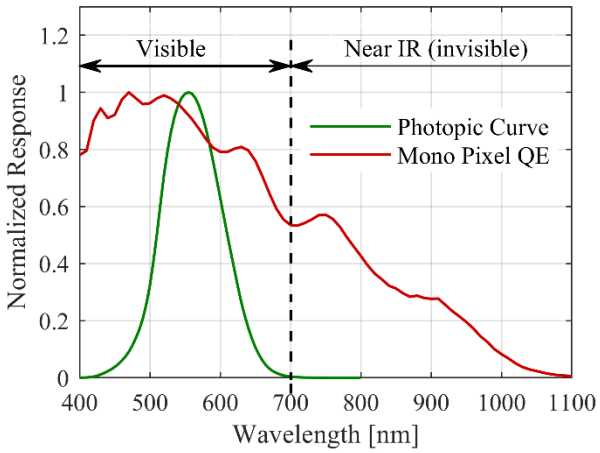

Figure 1 – Normalized plots of the HVS photopic curve and an example quantum efficiency (QE) curve of a monochrome CMOS image sensor.

Dual-Band Imaging

The different approaches to single-camera dual-band imaging are based on different combinations of color filters in the pixel array, camera filter, and processing pipeline.

Pixel Array Color Filters and Camera Filters

Most color CMOS image sensors are RGB sensors that use the traditional Bayer pattern color filter array (CFA) structure, where each 2×2 cell unit has one red (R), two green (G), and one blue (B) pixels, as shown in Figure 2(a). Example normalized quantum efficiency (QE) curves of an RGB sensor are shown in Figure 3(a). One may conclude from these curves that the RGB color filters are transparent to NIR light, starting from wavelength of about 850 nm, as QE curves of the three color channels in this band are similar.

Figure 2(b) presents an example CFA pattern of an RGB-IR image sensor. This pattern, when used with a DBF and a compatible pipeline, may be considered as the straightforward approach for dual-band imaging. In the configuration that is shown

in Figure 2(b), each 4×4 cell unit has eight G, four IR, two R and two B pixels. Example QE curves of an RGB-IR sensor are shown in Figure 3(b). The IR pixels include a filter that suppresses transmission of light in the visible band. Therefore, QE of the IR channel in the visible band is very low, but its QE in the NIR band is similar to that of the RGB channels. This channel is used as a reference to correct the NIR signal from the signals of the other color channels by subtraction of the NIR channel signal from the signals of the R, G, and B channels.

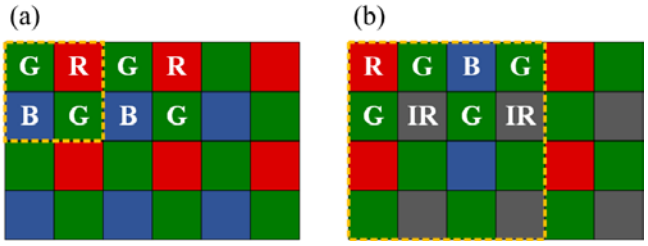

Figure 2 – Color filter array of (a) Standard Bayer RGB sensor and (b) RGB-IR sensor with a 4×4 kernel.

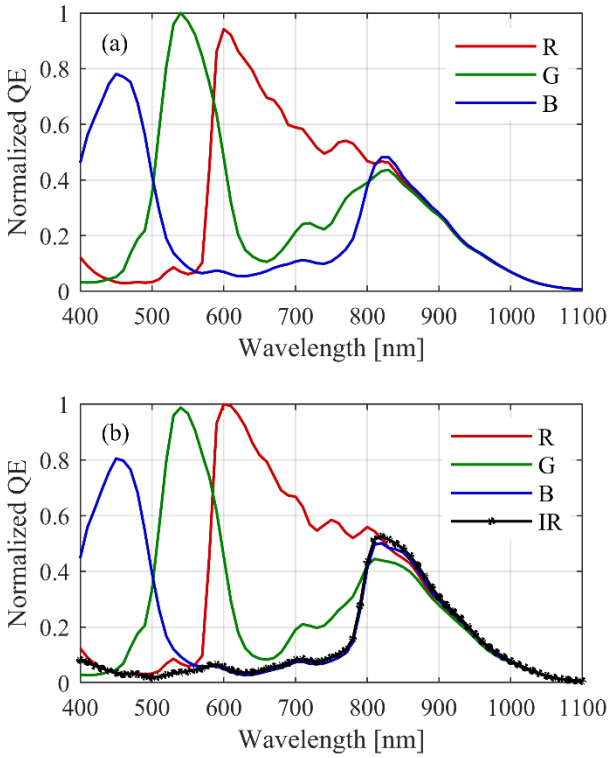

Figure 3 – Normalized QE curves of (a) RGB sensor and (b) RGB-IR sensor.

To eliminate NIR artifacts in the general case of visible-band imaging with an RGB sensor, an IRCF is placed in the path of the light to prevent NIR photons from reaching the image plane by absorption and/or reflection of infrared radiation. The blue curve in Figure 4 presents an example normalized transmission spectrum of a standard IRCF. One may conclude that this filter prevents photons with wavelength that is 700 nm and longer from reaching the image plane.

To exploit the advantage of a sensor with an RGB-IR CFA, it should be used with a DBF. The red curve in Figure 4 presents an example normalized transmission spectrum of a DBF. This filter has two pass-bands, where the first covers the visible-band and resembles a standard IRCF, and the second is a narrow pass-band in the NIR, which is around 850 nm in the example transmission curve in Figure 4.

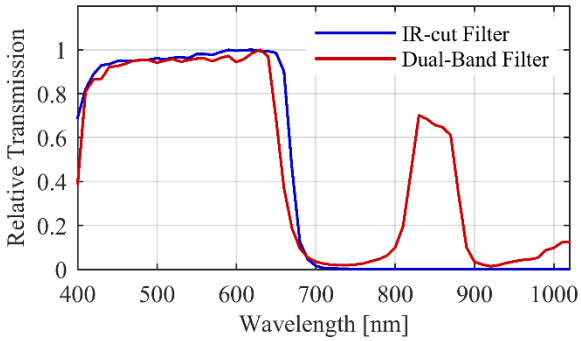

Figure 4 – Example relative transmission curves of an IRCF and a DBF with a pass-band in the visible and a narrow pass-band around 850 nm.

Color Imaging Pipeline

Figure 5(a) presents the main blocks in a standard imaging pipeline of RGB sensors. After black-level subtraction, raw image data is first processed by a demosaic block that produces an image in full color RGB format. Then, white balance is applied to properly render neutral colors. The color correction block multiplies the white-balanced RGB image data by a color-correction matrix (CCM) and produces an image in linear sRGB format. Lastly, the tone mapping block, which may apply standard gamma correction or a more complex tone mapping algorithm, produces an image in tone-mapped sRGB format.

Figure 5(b) presents the main processing blocks in an imaging pipeline that was developed for RGB-IR sensors [1]. Other RGB-IR pipelines have been proposed see, for example, the work by Teranaka et al. [2]. Although some blocks are similar to those that are found in the standard RGB pipeline, there are some differences between the pipelines because of the additional channel. The demosaic block must be replaced or modified to account for the NIR channel. The pipeline must include an IR subtraction block to enable utilization of the IR channel signal as a reference for correction of IR image artifacts. In other words, the standard pipeline is not suitable to use with RGB-IR sensors.

To minimize system complexity, this work aimed to develop a method that allows dual-band imaging with RGB sensors and a standard RGB pipeline. The only block that can be optimized to improve color reproduction when the sensor is exposed to NIR radiation is the color correction block, where the color correction matrix can be optimized to consider the increased signal offset due to absorption of NIR photons. To our knowledge, no similar approach has been presented before in the literature.

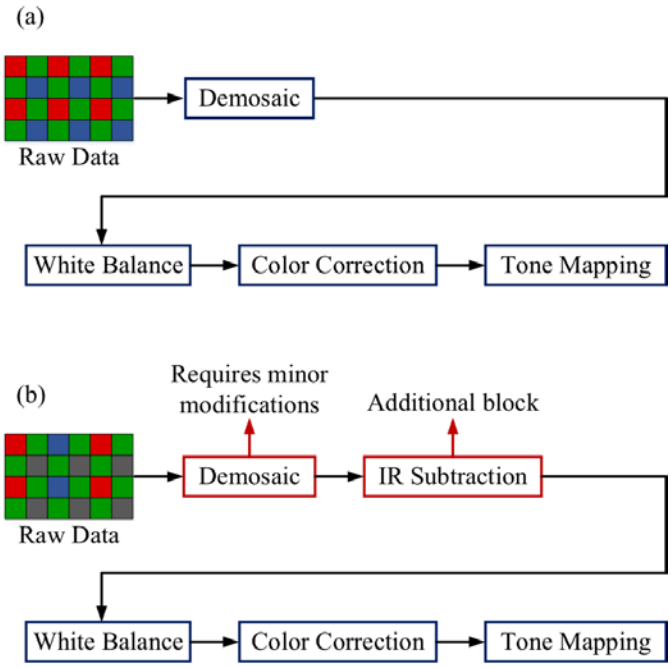

Figure 5 – Main blocks in the color processing pipeline of (a) standard RGB and (b) RGB-IR image sensors.

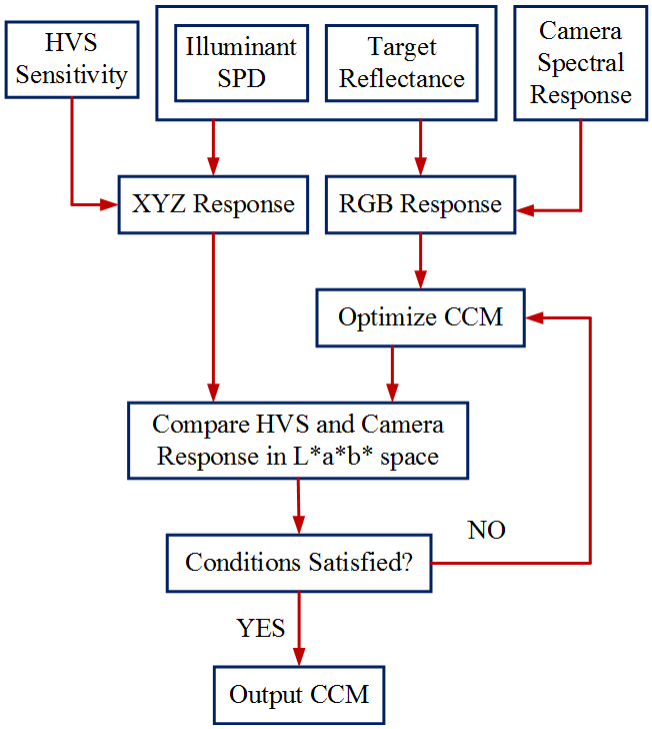

Figure 6 – Main blocks in the algorithm for CCM optimization. Camera sensitivity is determined from sensor QE and filter transmission. Color matching functions are used for HVS sensitivity.

CCM Optimization

Figure 6 presents a block diagram of an algorithm for CCM optimization. Input parameters include illuminant spectral power distribution (SPD), target reflectance, HVS color matching functions, and the camera spectral response. As tools for CCM optimization are typically developed for cameras with an RGB sensor and an IRCF, the typical target reflectance data set is given in a wavelength band that covers the visible band with small extensions to shorter and longer wavelengths. Camera spectral response profile is given by element-wise multiplication of channel QE by filter transmission curve. Figure 7(a) presents normalized camera spectral response curves for the case of an RGB sensor with an IRCF.

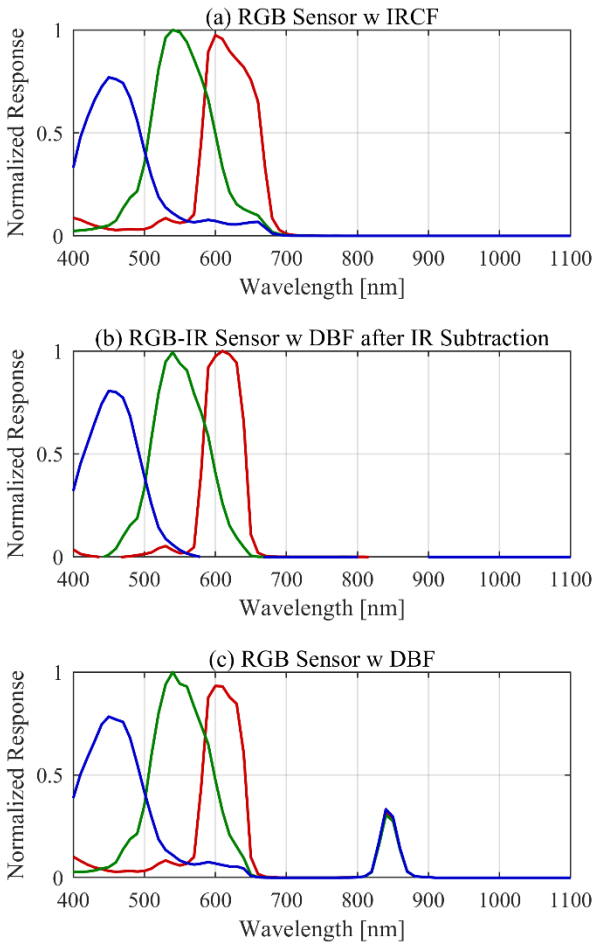

Figure 7 – The normalized spectral response of a camera in the case of: (a) RGB sensor with an IR-cut filter, (b) RGB-IR sensor with a DBF after IR subtraction, and (c) RGB sensor with a DBF.

The only change that is required when the CCM optimization tool is used for a camera with an RGB-IR sensor and a DBF is a step that performs subtraction of the spectral response of the IR pixel from the spectral response of the RGB pixels after element-wise multiplication by the DBF transmission curve. Figure 7(b) shows the normalized spectral response of the camera as obtained after this step is completed.

In a case of a camera that has an RGB sensor and a DBF, subtraction of the NIR signal is impossible. Therefore, the pixel spectral response curves are calculated, like in the case of an RGB sensor with an IRCF, by element-wise multiplication of channel QE by the DBF transmission curve. Normalized camera spectral response curves are shown in Figure 7(c). To consider the signal that is generated due to intentional exposure to NIR radiation, target reflectance data set must be given in a wavelength range that covers the visible and the NIR bands.

Experimental Results

Experimental work was done with two ON Semiconductor AR0237 image sensors [3]. These are front-side illuminated (FSI) image sensors with a 2 MP array and 3 µm pixel size. One of the sensors had a standard Bayer-pattern RGB CFA and the other had an RGB-IR CFA with a 4×4 kernel pattern. Two Sunex DSL945D lenses were used for image capture, one with a standard IRCF and one with a DBF with a narrow pass-band in the NIR around 850 nm.

For a realistic evaluation of the method, two image sets were captured in a car during day time. With all sensor and filter combinations, CCM was optimized for an illuminant with SPD of a black body at 5,000K as it approximates the SPD of the sun light during daytime. Target reflectance data set for the standard case included reflectance of the 96 color patches of a Digital Color Checker SG chart in the 380–780 nm range. An internal target data set with reflectance data from various materials, including foliage, in the range of 380–1,070 nm, was used for the case of an RGB sensor with a DBF.

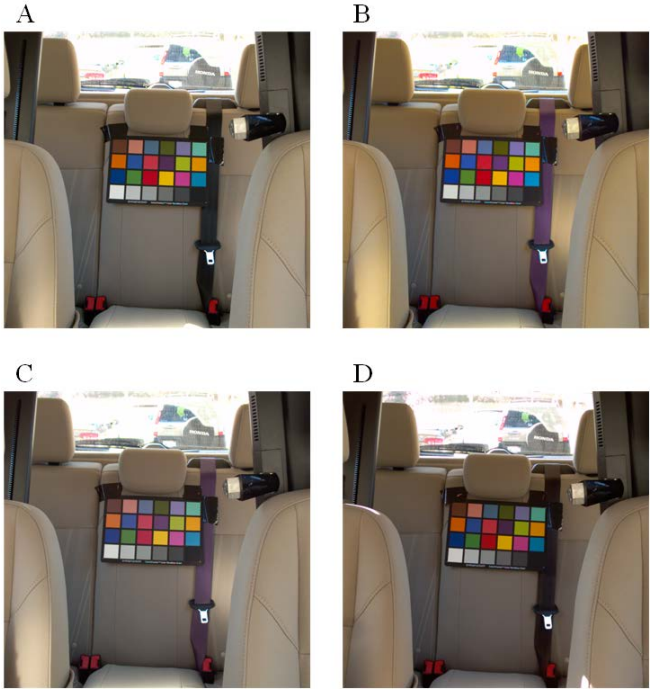

Figure 8 – Automotive in-cabin scene (back seat) images captured with: A – RGB sensor with an IRCF, B – RGB sensor with a DBF after color processing with a visible-NIR CCM, C – Raw image from B as processed with a CCM that was optimized for the visible band, and D – RGB-IR sensor with a DBF as processed with the RGB-IR pipeline.

Color Reproduction in Daytime Images

Figure 8 presents the first image set, which captured a Macbeth chart in the back seat. Image A was captured with an RGB sensor and an IRCF. Image B was captured with an RGB sensor and a DBF and then processed with a CCM that was optimized for the visible-NIR bands. Image C is based on the raw data of image B, however, processing was done with a CCM that was optimized only for the visible band. Image D was captured with an RGB-IR sensor and a DBF and then processed through the RGB-IR pipeline.

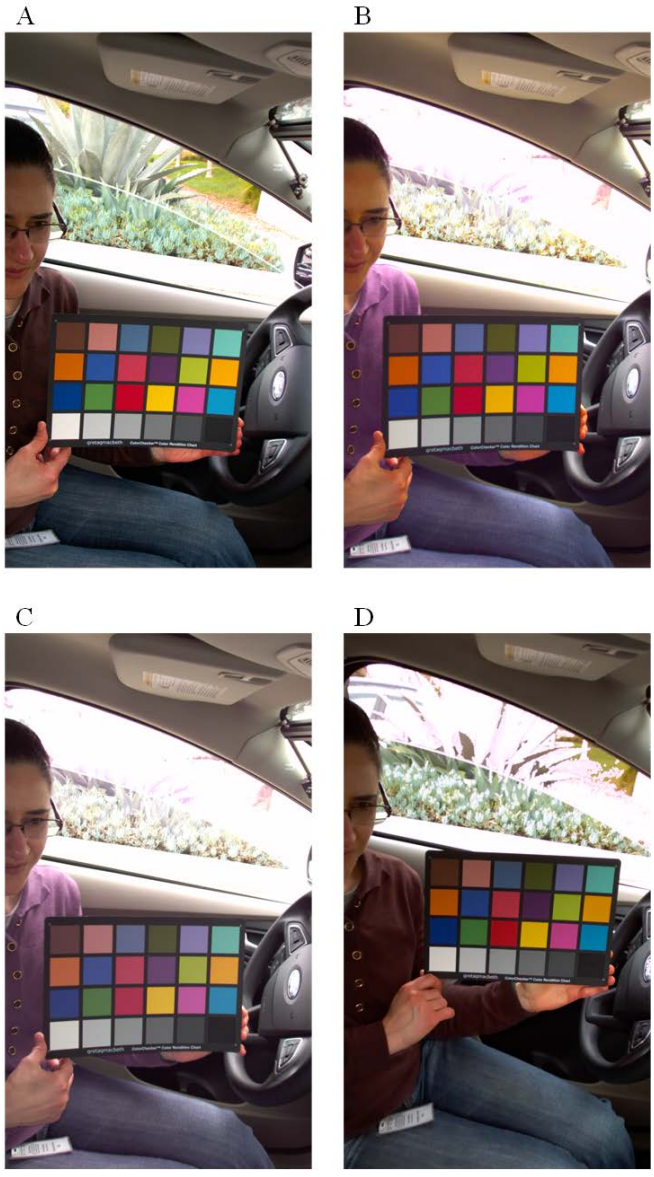

Figure 9 – Automotive in-cabin scene (driver seat) images captured with: A – RGB sensor with an IRCF, B – RGB sensor with a DBF after color processing with a visible-NIR CCM, C – Raw image from B as processed with a CCM that was optimized for the visible band, and D – RGB-IR sensor with a DBF as processed with the RGB-IR pipeline.

Colors of the Macbeth chart patches and the back seat fabric in image B appear, by qualitative evaluation, similar to those in image A. However, the seat belt, which is black in A appears purple in B. This is a result of the high reflectance in NIR of the seat belt material. Macbeth chart colors in image C appear duller and less saturated than in image B. Also in this image, the seat belt appears purple. In image D, the RGB-IR pipeline corrects the offset that is caused by NIR exposure and the seat belt appears black.

Figure 9 presents the second image set, which captured the driver seat, where image order is the same as in Figure 8. Colors of the Macbeth chart patches and the car interior in image B is qualitatively similar to those in image A. However, the color of the jeans appears somewhat purple and the color of the shirt appears purple instead of brown. The same color artifacts are also observed in image C and, like before, color saturation level in image C is lower than in image B. Color artifacts, which are produced by exposure to NIR photons, are corrected in image D by the RGB-IR pipeline.

To quantitatively evaluate color properties of the different images, Macbeth chart images were analyzed with the Colorcheck tool in the Imatest software v4.4.7 using reference data from an X-Rite MCC post Nov 2014 chart under a D50 illuminant. Figure 10 presents analysis results for color saturation and mean color difference, ΔC.

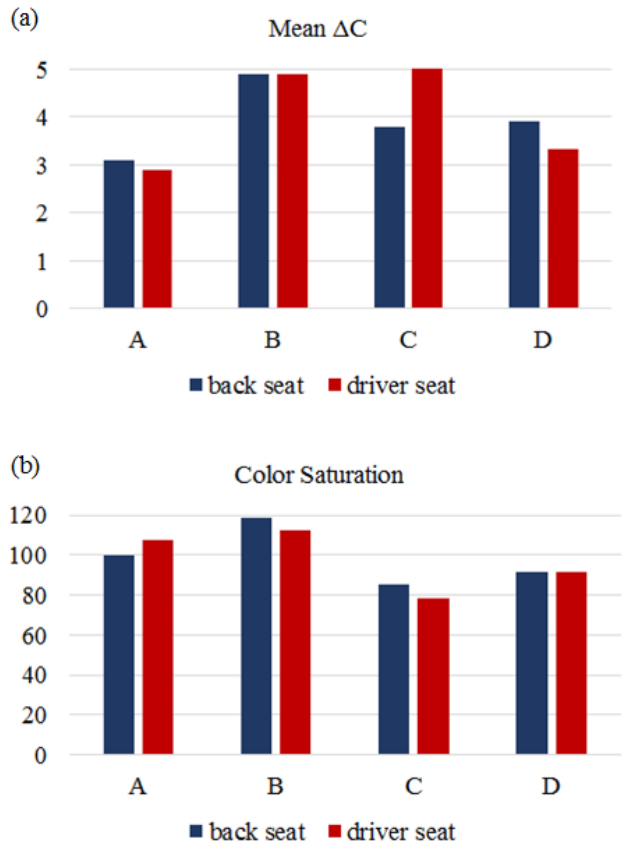

Figure 10 – Color properties of the Macbeth chart images in images A–D in Figure 8 and Figure 9. Mean color difference, which is shown in (a), should be as low as possible. With both metrics, image A, which was captured with an RGB sensor and an IRCF, achieves the best results, as expected. Color saturation, which is shown in (b), should ideally be as close as possible to 100%.

Color difference should be, in general, as low as possible. Though, to minimize color noise artifacts in low-light conditions, the algorithm for CCM optimization trades off color accuracy for noise-gain. Figure 10(a) shows that, as expected, the two images that were captured with an RGB sensor and an IRCF achieve the lowest values.

One of the conditions that are set in the tool for CCM optimization is to achieve color saturation level that is as close as possible to 100%. One may conclude from Figure 10(b) that color saturation in the images that were captured with an RGB sensor and an IRCF, i.e., A in the plot, is the closest to 100%. The plot confirms that color saturation is significantly higher when images that are captured with an RGB sensor and a DBF are processed with a CCM that was optimized for the visible and NIR bands. Color saturation in the RGB-IR images is about 90%, which is slightly lower than desired. In bright scene conditions, the optimal color saturation level for image pleasantness is 110% [4]. Therefore, a CCM that is optimized for the visible-NIR bands is preferred over a CCM that is optimized only for the visible band for images that are captured with an RGB sensor and a DBF.

High NIR Reflectance Artifacts

The RGB-IR pipeline includes two branches: a visible color pipeline, which was described in a previous section, and a monochrome NIR pipeline. The input to the NIR pipeline is the information that is collected by the NIR pixels, which constitute 25 percent of the pixels in the array. Figure 11 presents the output after the same raw image, which was captured with and RGB-IR sensor and a DBF is processed through both branches of the RGB-IR pipeline. The brightness of the foliage outside the car, the shirt and some of the Macbeth chart patches indicates that these materials have high reflectance in the NIR. This confirms that the color artifacts that were obtained in the images that were captured with the RGB sensor and a DBF are a result of an increased offset due to high NIR signal.

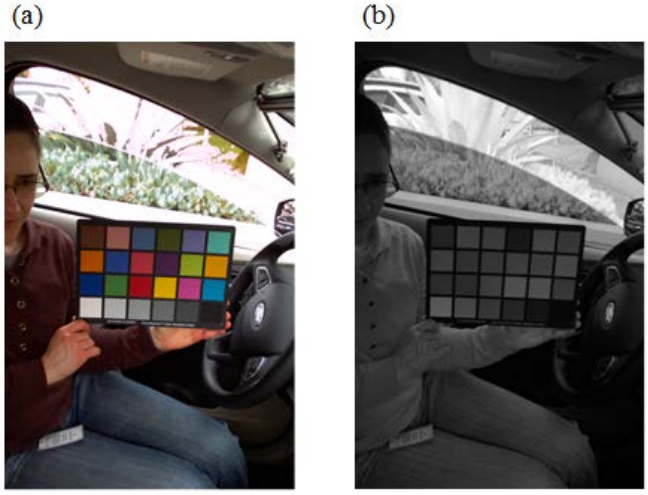

Figure 11 – Output image from (a) the visible color branch and (b) the monochrome NIR branch of the RGB-IR pipeline. The brightness of the shirt, some of the patches in the Macbeth chart, and the foliage in image (b) indicates that the reflectance of these materials in the NIR band is high.

Enhancement in signal offset in image regions with objects with high NIR reflectance manifest in shift of color towards purple. Figure 12 shows the process that leads to this outcome in three steps of the pipeline: (a) raw image, (b) image after white balance and (c) image after color-correction and tone mapping.

The plots in Figure 12(a), (b), and (c) represent the column average signal in the region that is surrounded by a red dashed-line rectangular in the image above each plot. The red rectangular covers all the grey-scale patches of the Macbeth chart and a region in the seat belt. The image in Figure 12(a) is the raw image before black-level subtraction. One may conclude that in all grey-scale patches, the green channel has the highest signal level among the three color channels. Signal level of all color channels in the seat belt region of the image is nearly similar and higher than their signal levels in the black patch. If the sensor was not exposed to NIR photons, signal levels in the seat belt region would be similar to those in the black patch region.

Figure 12(b) presents the image after black-level subtraction, white balance, where red and blue signal levels are digitally amplified to obtain equal signal levels on the grey-scale patches, and conversion to a standard 24-bit bitmap format. The seat belt region appears purple because the red and blue signals were amplified, but the green signal was not. Figure 12(c) shows the image after full processing through the color pipeline, including color correction and tone mapping. These processing steps enhance color saturation and the purple artifact becomes more noticeable.

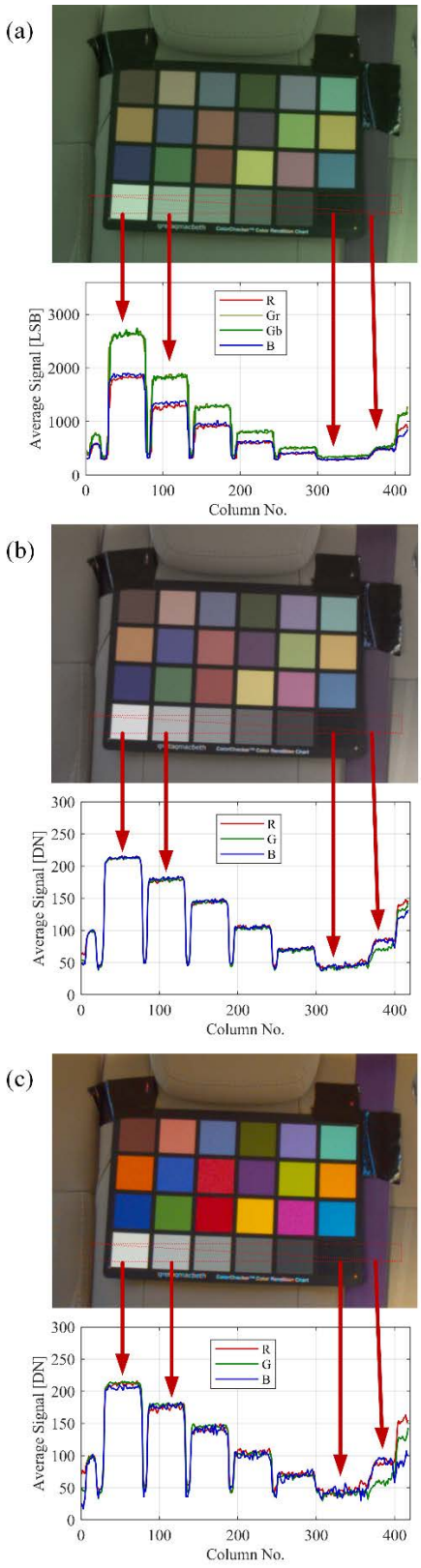

Figure 12 – The process that results in appearance of purple artifacts in images of objects with high NIR reflectance. All plots show average column signal in the image area that is surrounded by the red rectangular. (a) Raw image; (b) White-balanced image; (c) Image after color-correction and tone mapping.

Conclusion

This work presented four single-camera methods for dual-band imaging in the visible and NIR bands. A summary of the work is shown in Table 1.

Table 1 – Summary of methods for dual-band imaging.

	CFA	Filter	CCM	Spatial	Color	Complexity
A	RGB	IRCF	VIS	High	High	High
B	RGB	DBF	VIS-NIR	Good	Medium	Low
C	RGB	DBF	VIS	Good	Low	Low
D	RGB-IR	DBF	VIS	Low	Good	Medium

Method A achieves the highest score on image quality metrics, which include spatial resolution and metrics related to color reproduction. However, system complexity is high as it requires a mechanical feature that removes the filter at nighttime to enable NIR imaging.

Method B exhibits color artifacts in images of objects that have high reflectance in the NIR. In addition, it is likely to result in some degradation in spatial resolution metrics as NIR photons can travel long distances in the silicon substrate, which increases crosstalk and leads to degradation in spatial resolution. However, its biggest advantage is system simplicity as it can be implemented in a standard color imaging pipeline.

Method C is similar to B, but color reproduction metrics are inferior to B because of loss of color saturation.

Method D corrects color artifacts that are caused by NIR exposure. However, it requires to modify or replace the color imaging pipeline because it is not compatible with the standard one. Furthermore, use of this method is likely to result in degradation in spatial resolution and related metrics as there are less pixels that collect information in the visible band and in the NIR band.

To conclude, with automotive in-cabin monitoring and surveillance applications, if color is not the primary information required by the system, and if there is no need in simultaneous dual-band imaging, method B is the preferred one as it satisfies performance requirements without an increase in system complexity.

Acknowledgment

The authors would like to thank James Gross, Lin Lin, and Leo Lautenschlager for their technical assistance.

References

[1] ON Semiconductor, *AND9492/D RGB-IR Sensors and Image, Product Datasheet,* 2016.

[2] H. Teranaka, Y. Monno, M. Tanaka and M. Okutomi, "Single-Sensor RGB and NIR Image Acquisition: Toward Optimal Performance by Taking Account of CFA Pattern, Demosaicking, and Color Correction," in *Electronic Imaging*, 2016.

[3] ON Semiconductor, *AR0237CS 1/2.7-inch 2.1 Mp/Full HD, Product Datasheet,* 2018.

[4] B. W. Keelan, R. B. Jenkin and E. W. Jin, "Quality versus color saturation and noise," in *Proc. SPIE*, 2012.

Author Biography

Orit Skorka received her BSc from Ben-Gurion University of the Negev, Israel, in 2001, her MSc from the Technion IIT, Israel, in 2004, and her Ph.D. from the University of Alberta, Canada, in 2011, all in Electrical and Computer Engineering. She joined Aptina in 2013 and is now with the Image Sensor Group at ON Semiconductor working on pixel characterization and image quality of CMOS image sensors for automotive, security and other imaging applications.

Paul J. Kane received a B.S. in Physics from the University of Scranton and an M.S. in Optics from the University of Rochester. He was a scientist at the Kodak Research Laboratories for 28 years, working primarily in the areas of imaging science and optics. His projects there included system modeling and simulation, image processing for OLED displays, 3D imaging and light scattering from small particles. In 2015 he joined ON Semiconductor as an Algorithm Design Engineer, focusing on automotive and security applications. Mr. Kane holds 35 U.S. patents in the areas of algorithms, display technologies and solid state lighting. He is a Senior Member of SPIE.

Radu Ispasoiu is a senior manager of pixel R&D and image quality at ON Semiconductor ISG (since 2014). He has held engineering management and lead R&D positions in the Silicon Valley optoelectronics technology industry for more than 18 years. He holds a PhD in Physics (1996) with focus on semiconductor optoelectronic device study from the University of Oxford, UK.

JOIN US AT THE NEXT EI!

IS&T International Symposium on

Electronic Imaging

SCIENCE AND TECHNOLOGY

Imaging across applications . . . Where industry and academia meet!

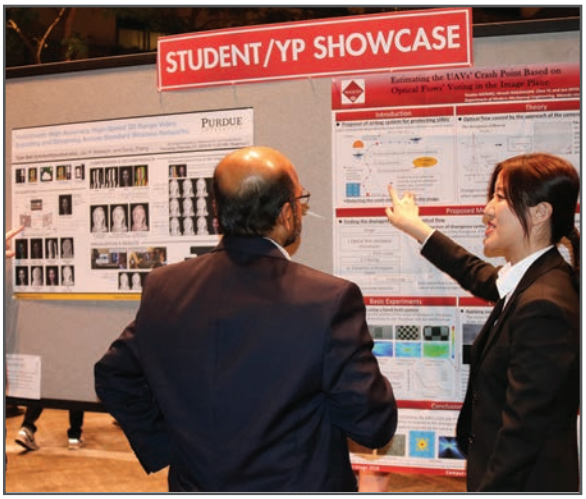

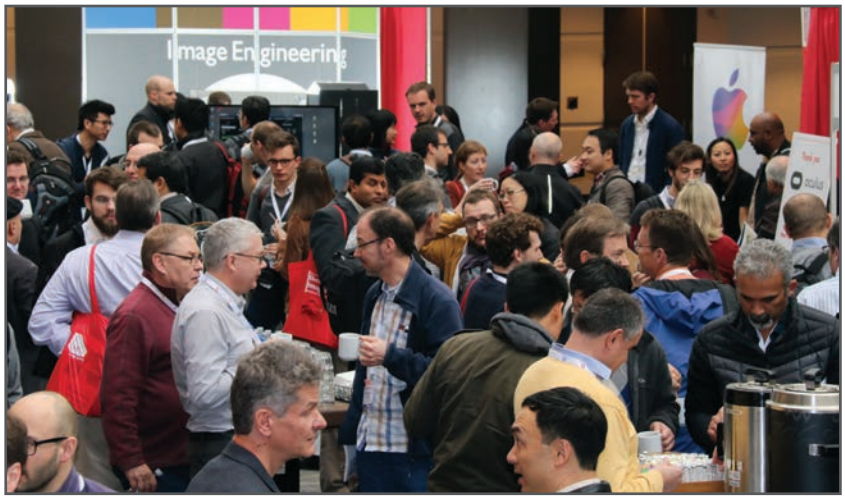

• SHORT COURSES • EXHIBITS • DEMONSTRATION SESSION • PLENARY TALKS •
• INTERACTIVE PAPER SESSION • SPECIAL EVENTS • TECHNICAL SESSIONS •

www.electronicimaging.org

IS&T
imaging.org